NANO LETTERS

pubs.acs.org/NanoLett Letter

Calibrating Out-of-Equilibrium Electron−Phonon Couplings in Photoexcited MoS_2

Xin-Bao Liu,[‖] Shi-Qi Hu,[‖] Daqiang Chen, Mengxue Guan, Qing Chen, and Sheng Meng*

Cite This: *Nano Lett.* 2022, 22, 4800−4806 Read Online

ACCESS | Metrics & More | Article Recommendations | Supporting Information

ABSTRACT: Nonequilibrium electron−phonon coupling (EPC) serves as a dominant interaction in a multitude of transient processes, including photoinduced phase transitions, coherent phonon generation, and possible light-induced superconductivity. Here we use monolayer MoS_2 as a prototype to investigate the variation in electron−phonon couplings under laser excitation, on the basis of real-time time-dependent density functional theory simulations. Phonon softening, anisotropic modification of the deformation potential, and enhancement of EPC are observed, which are attributed to the reduced electronic screening and modulated potential energy surfaces by photoexcitation. Furthermore, by tracking the transient deformation potential and nonthermal electronic population, we can monitor the ultrafast time evolution of the energy exchange rate between electrons and phonons upon laser excitation. This work provides an effective strategy to investigate the nonequilibrium EPC and constructs a scaffold for understanding nonequilibrium states beyond the multitemperature models.

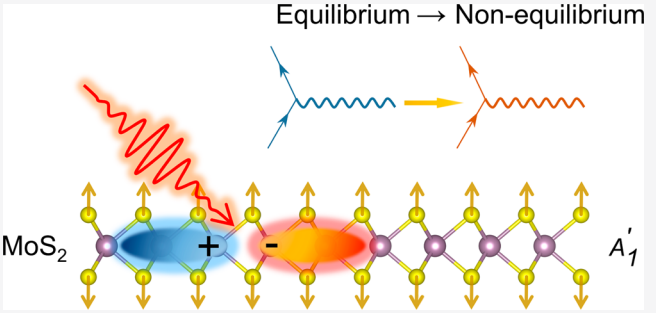

KEYWORDS: *nonequilibrium states, electron−phonon coupling, time-dependent density functional theory, ab initio calculations, dynamically screened potential*

Electron−phonon coupling (EPC) dominates a variety of materials properties such as electrical resistivity, heat capacity, and the transition temperature of superconductors.[1] This old tree sprouts new buds in a wide range of nonequilibrium conditions such as nonradiative recombination and thermalization of photocarriers in semiconductors,[2,3] polaron formation,[4] photoinduced phase transitions,[5,6] coherent phonon generation,[7−9] and possible light-enhanced superconductivity.[10,11] The nonequilibrium EPC under photoexcitation offers new possibilities to control quantum materials such as controlling topological properties, guiding directional phase transitions, and manipulating carrier lifetimes.[12−20] Nevertheless, despite its great potential, a clear picture of the EPC in excited states is still lacking. In order to understand these nonthermal phenomena, quantitatively calibrating the electron−phonon scattering processes between photoexcited electrons and the lattice is necessary.

In the literature quasi-thermal descriptions have usually been employed to quantify the relaxation processes associated with laser excitation. On the basis of the standard Bloch−Boltzman−Peierls formulas, the two-temperature model (TTM) has often been used to depict the energy exchange between the photoexcited electrons and the lattice in metals under photoexcitation.[21−23] The nonequilibrium EPC was characterized by the equilibrium electron−phonon coupling matrix element g_{ij} and the quasi-thermal occupations of electrons and phonons, which are described by the Fermi−Dirac and Bose−Einstein distributions with the respective effective temperatures. However, there exist a few severe limitations with these quasi-thermal descriptions. (i) The assumption of a quasi-thermal equilibrium in a given subsystem is questionable. (ii) The constant value of matrix elements for electron−phonon scatterings is suspicious under nonequilibrium conditions. The trouble of slow thermalization within the phonon subsystem can be partially solved by a generalized TTM together with time-dependent Boltzmann transport equations.[23−27] In contrast, the constant value of EPC matrix elements under photoexcitation has, to our surprise, yet to be checked. The EPC matrix element, g_{ii}, namely the deformation potential (DP) of a given electronic state with respect to specified phonon modes, describes the change in electronic energy level upon the unit amplitude of phonons, thus depicting the effective potential experienced by electrons in a unit cell.[28] It has been shown that an effective electron−electron interaction and electron−phonon interac-

Received: March 18, 2022
Revised: May 27, 2022
Published: June 1, 2022

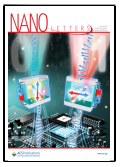

https://doi.org/10.1021/acs.nanolett.2c01105
Nano Lett. 2022, 22, 4800−4806

tion could be modulated upon photoexcitation.[29−31] The effective "screening" as well as the EPC matrix elements would change due to transient perturbation of the laser field.

Recent works have shown that EPC matrix elements could be mapped by monitoring the time-resolved electronic structure and the coherent phonon dynamics,[32−35] whereas the mechanism of nonequilibrium electron−phonon coupling is still obscure, due to the difficulty in loading a single coherent phonon mode elaborately via photoexcitation. Therefore, there is an urgent need to investigate photoinduced nonequilibrium EPC matrix elements using first-principles calculations, which is the basis of clarifying the effective coupling strength between the laser-excited electrons and specific phonon modes.

In this work we calculate the nonequilibrium EPC matrix elements and EPC strength under laser excitation in monolayer MoS_2 (1L-MoS_2), targeting a clear description of the energy exchange between photoexcited electrons and the lattice. Our first-principles molecular dynamics (MD) simulation via time-dependent density functional theory (TDDFT)[36] and Ehrenfest dynamics shows that the photoinduced charge transfer could reduce the electronic screening and modulate the EPC matrix elements on an ultrafast time scale. By means of modulating the potential energy surface, the photoexcitation could enhance the EPC in monolayer MoS_2. In addition, we quantify the electron−phonon energy exchange rates after the femtosecond laser illumination to elucidate the energy relaxation processes from the photocarriers to high-energy optical phonons. Our work is beneficial for a quantitative understanding of the emerging nonequilibrium phenomena mediated by electron−phonon couplings, and it provides a new perspective toward utilizing laser-modulated quantum materials.

RESULTS

The calculations are performed on the basis of first-principles TDDFT using a time-dependent *ab initio* package (TDAP).[37−39] To investigate the nonequilibrium EPC, we first quantify the excitation of electrons and phonons upon laser illumination. The photon energy was set as $\hbar\omega = 1.7$ eV in accordance with the calculated band gap of 1L-MoS_2, and the maximum of the laser electric field is located at $t_0 = 50$ fs. (More details about the computational method can be found in the Note 1 in the Supporting Information.) The laser-induced evolution of electronic population is monitored to study the dynamics of the electron subsystem. The occupation of the conduction band minimum (CBM) increases rapidly and reaches a maximum at $t_0 = 50$ fs and then slightly decays to a constant value (Figure 1e). Resonant excitations, combined with the valley structure of conduction bands, give rise to the electronic excitation mainly located in the K valley (Figure 1c). In the meantime, the atomic displacements along the A'_1 phonon mode are launched by the laser excitation (Figure 1b,f). The band energy at the CBM starts to oscillate with a period of $T \approx 81$ fs (Figure 1g), close to the period of the A'_1 phonon in the ground state (80.2 fs). In addition, the high-frequency oscillation ($T \approx 5$ fs) of the energy band may result from the beating formed by the first-order and second-order laser dressed charge density oscillation (A more detailed discussion about this oscillation can be found in Note 11 in the Supporting Information.) These results show the effect of transient electron−phonon couplings between electron and phonon subsystems during photoexcitation. By means of the nonequilibrium EPC, the photoexcited electrons provide the driving forces for the coherent phonon generation.

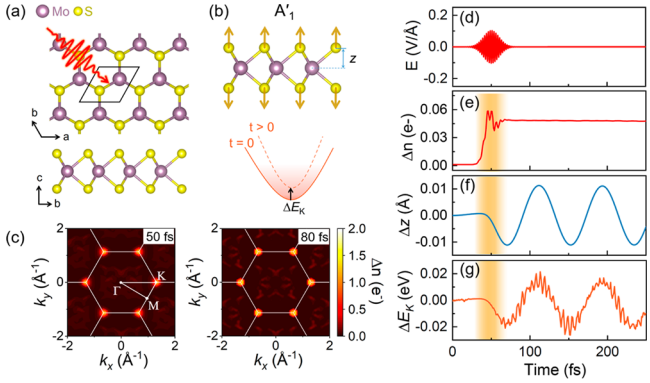

Figure 1. Laser-induced excitation of electrons and phonons. (a) Schematics of light-illuminated 1L-MoS_2 and its atomic structure. (b) Schematics of the A'_1 mode (top panel) and the energy shift in the K valley (bottom panel). (c) Occupation distribution of photoexcited electrons at $\hbar\omega = 1.7$ eV excitation under a laser intensity of 2.5 mJ/cm^2, resulting in a photocarrier density $n \approx 5.7 \times 10^{13}$ cm^{-2}. The left panel depicts the distribution under the strongest electric field of the laser pulse (50 fs), while the right panel is the corresponding distribution after the laser pulse vanishes (80 fs). The latter exhibits a slight polarization along the k_x direction. (d) Electric field profile of the laser pulse. (e) Time-resolved occupation of photoexcited electrons in the conduction band. (f) Displacements of sulfur atom Δz (blue) and (g) the band energy shift ΔE_k (orange) of the k point in Brillouin zone under photoexcitation. The yellow shadows schematically indicate the intensity of the laser pulse.

After the end of the laser pulse, the electronic occupation of K valley remains unaltered and this long-lived occupation will persist for a long time (over 80 ps according to the experimental measurements), until it is depleted by radiative electron−hole recombination.[9,40,42] In comparison with the experimental condition, the decays of electronic occupation and optical phonons are partially suppressed here due to the limited scattering channels included in the simulations, while this simplification provides a great convenience for investigating the transient EPC between the photoexcited carriers and high-energy optical phonon modes, mainly the A'_1 phonon.

Through projecting the atomic displacements onto the complete set of phonon eigenmodes, we obtain the mode-resolved vibrational amplitude in photoexcited 1L-MoS_2. Upon laser excitation, the synchronized oscillation of Δz (the atomic displacement along the surface normal z direction) and ΔE_k (the shift of electronic energy level at the k point in the Brillouin zone) indicate that light excitation is still in the perturbation regime (Figure 1f,g). Further analysis shows that A'_1 and E' are the two primary phonon modes being stimulated by the laser pulse. The amplitude of A'_1 is 3.75 times larger than the E' mode (see Figure S1), indicating that the A'_1 phonon is dominant. Furthermore, the deformation potential of E' is close to zero at the K valley; therefore, it hardly contributes to the EPC. Thus, we focus only on the dominant A'_1 mode hereafter (Supporting Information Note 2).

On the basis of the above analysis on photoexcited electrons and phonons, we turn to evaluating the photoinduced EPC of the transient states. In principle, the electron−phonon coupling constant of the phonon mode ν at q under the ground-state condition is given by[43]

https://doi.org/10.1021/acs.nanolett.2c01105
Nano Lett. 2022, 22, 4800−4806

$$\lambda_{q\nu} = \frac{1}{N(\varepsilon_F)\omega_{q\nu}} \sum_{ij} \sum_{k} |g_{ij}^{q\nu}(k, k+q)|^2 \times \delta(\varepsilon_{k+q,i} - \varepsilon_F)\delta(\varepsilon_{k,j} - \varepsilon_F) \quad (1)$$

where $g_{ij}^{q\nu}(k,k+q)$ is the electron−phonon coupling matrix element, $N(\varepsilon_F)$ is the density of states near the Fermi level, and $\omega_{q\nu}$ is the phonon frequency. To evaluate the coupling strength between the photocarriers and phonons, we adopt the two-chemical-potential approach, which has been shown to correctly explain the excitation of coherent phonons.[9,41,44,45] Since the photoexcited electrons/holes scale with the laser intensity, two Fermi surfaces on the CBM and valence band maximum (VBM) at the K valley, respectively, are defined. The locations of the two Fermi surfaces are determined by the respective occupation of photoexcited electrons and holes (see more details in Note 8 in the Supporting Information). Here in photodoped MoS_2, the EPC mainly stems from intraband transitions between states in the vicinity of the Fermi surfaces: namely, $g_{ii}^{q\nu}(k,k+q)$ in the K valley of CBM and VBM.[46] Thus, the EPC constant $\lambda_{q\nu}$ under laser excitation is determined by two factors: (i) the intraband electron−phonon coupling matrix elements $g_{ii}^{q\nu}$ and (ii) the density of states near the Fermi levels.

By monitoring the variations of energy band and projected phonon amplitude, we could extract the EPC matrix elements from simulated trajectories upon photoexcitation. In Figure 2a the energy variations of CBM and out-of-plane atomic displacements of the sulfur atoms are shown at four representative instances. The gray line corresponds to the energy band of the undistorted structure at the time $t < 0$. When the ions move along the direction of phonon eigenmode displacement, the prominent shift of the energy band (ΔE) is proportional to the atomic displacements of sulfur atoms (Δz) (right panel of Figure 2a), which scales with the projected phonon amplitude of the A'_1 mode (Δu). Then the EPC matrix element can be extracted from the gradient of ΔE to Δu

$$g_{ii}^{A'_1}(k, k) = \sqrt{\frac{\hbar}{2m_0\omega_{A'_1}}} \frac{\partial E_k}{\partial u} \quad (2)$$

where E_k is the band energy at the momentum k point, u is the projected phonon amplitude, and m_0 and $\omega_{q\nu}$ are the reference mass and the phonon frequency, respectively. To enhance the numerical stability, we average the amplitude of band energy and atomic displacements by fitting the oscillations of ΔE_k and Δu in a time period of several cycles (~200 fs) with a cosine function (Note 3 in the Supporting Information). By employing the above method in a Ehrenfest molecular dynamics simulation of 1L-MoS_2 with a single coherent A'_1 mode, we extract the EPC matrix elements of CBM and VBM in the ground and excited states. The ground-state g_{ii} values agree well with the results calculated by density functional perturbation theory (DFPT) using the Quantum Espresso package[47,48] (Note 4 in the Supporting Information).

The successful characterization of photoexcited electrons and phonons enables us to extract the nonequilibrium EPC matrix elements under photoexcitation. The time window is selected from ~70 fs, when the coherent phonons begin to vibrate, to 250 fs. In Figure 2c we compare the variations of nonequilibrium intraband EPC matrix elements g_{ii} of the valence band and conduction band, with the g_{ii} values being extracted from the ground-state molecular dynamics launched with the same initial structure. Obviously the 6-fold symmetry is broken in the photoexcited states, due to the influence of the in-plane E′ mode, whose g_{ii} value also breaks the 6-fold symmetry (Note 10 in the Supporting Information). The amplitude of g_{ii} is enlarged over almost the whole Brillouin

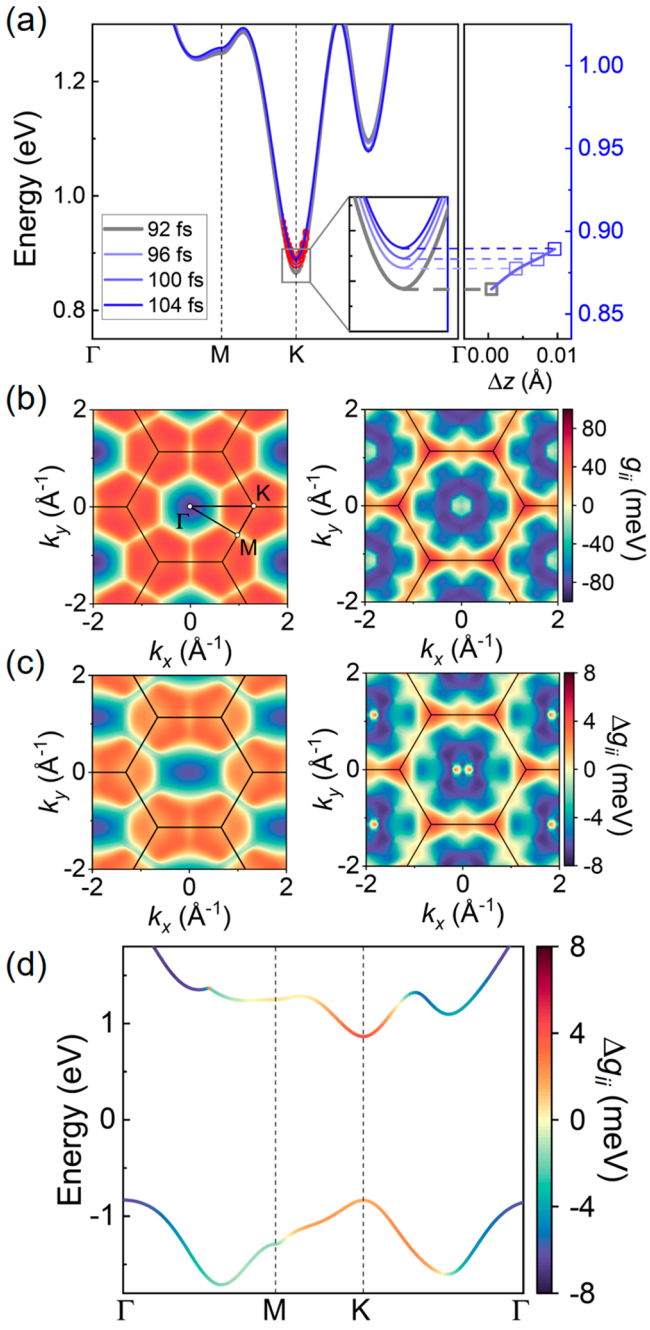

Figure 2. Evaluation of the out-of-equilibrium electron−phonon coupling matrix elements. (a) The left panel shows the variations of energy bands in several snapshots at t_0 = 0 fs, t_1 = 92 fs, t_2 = 100 fs, and t_3 = 104 fs. Red dots overlaid on the band structure indicate the electronic occupation excited by the laser pulse. The inset shows the amplification of energy band variations in the K valley. The right panel shows the band energy as a function of the corresponding displacements of sulfur atoms (Δz). (b) The ground-state g_{ii} values of the valence (left panel) and conduction (right panel) bands in the reciprocal space. (c) Variations of g_{ii} under light excitation in comparison with the ground state. (d) Corresponding variations of g_{ii} along the high-symmetry points.

https://doi.org/10.1021/acs.nanolett.2c01105
Nano Lett. 2022, 22, 4800−4806

zone, and the variation Δg_{ii} resembles g_{ii} in the ground state. Along the high-symmetry k-points path Γ−M−K−Γ, we find that g_{ii} is amplified at the K valley in both the CBM and VBM (Figure 2d), which is exactly the location of photoexcited electrons/holes. This increase in EPC matrix elements may strengthen the coupling between the excited electrons/holes and the A'_1 mode in 1L-MoS_2.

To figure out why photoexcitation alters the g_{ii} value, we calculate the modulation of the phonon frequency of the A'_1 mode and potential energy surface (PES) resulted from laser excitation. In comparison with the ground-state PES, the photoexcited PES is more flat and asymmetrical, which will lead to the softening of the A'_1 mode and the modulation of the deformation potential. As shown in the top panel of Figure 3a, the softening of the A'_1 mode basically scales with the

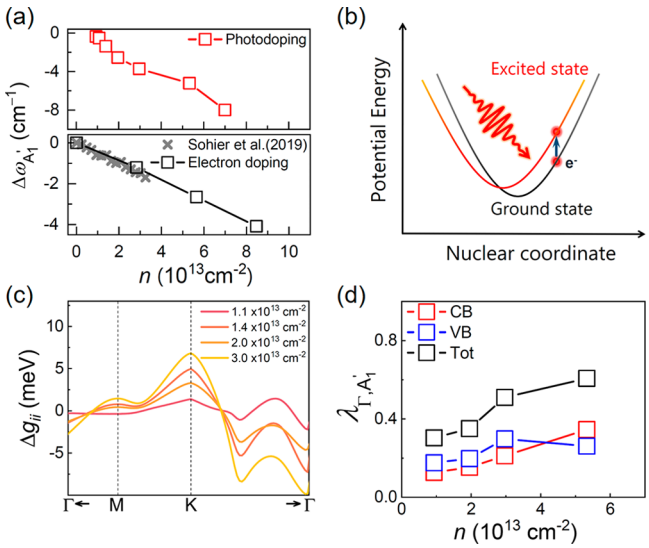

Figure 3. Modulation of electron−phonon coupling with different photoexcited carrier densities. (a) Softening of the A'_1 mode with various photoexcited carrier densities (red) and electron dopings (gray). The Raman spectral data (gray cross) are taken from ref 46. (b) Schematics of laser-induced variation in PES. The variations are exaggerated to make it more intuitive. The practical variations in PES are plotted in Figure S5. (c) Laser-induced variations of g_{ii} of the A'_1 mode under different photoexcited carrier densities in comparison with that in the ground state. (d) The corresponding electron−phonon coupling constant λ_{Γ,A'_1} of photoexcited monolayer MoS_2 as a function of photocarrier density.

density of photoexcited carriers. For comparison, we also calculate the phonon softening resulting from electron doping using a ground-state nonadiabatic molecular dynamics simulation, as shown in the bottom panel of Figure 3a. The latter is in very good agreement with experimental data (gray crosses).[46] The similar trend signifies a similar mechanism on EPC enhancement: namely, the reduced screening of electrons.

The softening of the A'_1 mode and anharmonic PES are closely related to the ultrafast charge transfer and reduction in electronic screening.[28,42,49] To elucidate the origin of EPC enhancement, we employ an analysis of the charge transfer and dielectric function under photoexcitation. The population of photoexcited electrons, as shown in Figure 2a, concentrated in the K valley (also in Figure 1e) can change the charge density distribution, thus modulating the electronic screening. More detailed analyses show that photoexcitation drives the charge transfer from the 4d orbital of Mo atoms to the 4p orbital of Se atoms (Figure S4). On the other side, the EPC matrix element can be related to the screening by[28]

$$g_{ij\nu}(\boldsymbol{k}, \boldsymbol{q}) = \left(\frac{\hbar}{2N_p M_\kappa \omega_{q\nu}}\right)^{1/2} \boldsymbol{q}\cdot e_{k\nu}(\boldsymbol{q}) \frac{V_\kappa(\boldsymbol{q})}{\varepsilon(\boldsymbol{q}, \omega_{\boldsymbol{q}\nu})} \tag{3}$$

where $\left(\frac{\hbar}{2N_p M_\kappa \omega_{q\nu}}\right)^{1/2}$ is the normalization factor of EPC in a unit cell. $\boldsymbol{q}\cdot e_{k\nu}(\boldsymbol{q})$ is the inner product of the wave vector q and the polarization of the phonon mode. $\frac{V_\kappa(\boldsymbol{q})}{\varepsilon(\boldsymbol{q}, \omega_{\boldsymbol{q}\nu})}$ is the "effective" dynamically screened potential experienced by electrons upon the displacement of the nuclei. Macheda et al. and Miller et al. also shown that the EPC is inversely proportional to the dielectric screening.[55,56] More intuitively, the effective potential felt by conduction band electrons can be written as

$$V_{\text{eff}}(\boldsymbol{q}, t) = V_{\text{ext}}(\boldsymbol{q}, t) + V_{\text{e-e}}(\boldsymbol{q}, t) \tag{4}$$

The electronic screening, corresponding to the electron−electron Coulomb interactions, are reduced by photoexcitation due to introduce the e/h pairs in the electron gas, which is consistent with previous works.[50,51] This reduction can give rise to an enhancement of the effective potential between the electrons and positively charged ions: namely, the EPC. Here we calculate the dielectric constant consisting of the electronic and ionic contributions. The dielectric constant $\varepsilon_\parallel$ is reduced from 5.72 in the ground state to 5.44 in the photoexcited state (approximately a 5% reduction, which is close to the enhancement magnitude of the g value, 6.3%). For more details about the dielectric constant of the photoexcited state see Note 6 in the Supporting Information. These results suggest that the photoinduced charge transfer will reduce the electronic screening to A'_1 mode, thus enhancing the EPC.

To investigate the relationship between the nonequilibrium EPC and laser excitation, we also calculate the variations of g_{ii} with different photocarrier densities. The amplitude of g_{ii} is enhanced at the K valley (Figure 3c). The amounts of these variations show a positive association with the photoexcited carrier $n \approx 10^{13}$ cm^{-2}. From the above discussion, the EPC constant of the A'_1 mode at the Γ point is evaluated as shown in Figure 3d, which basically grows linearly with the photoexcited carrier density. Overall, as the laser intensity increases, both the EPC matrix elements and density of states are enlarged and therefore the EPC constant increases. Therefore, we conclude that light excitation can enhance the EPC in monolayer MoS_2.

On the basis of the above analysis of the EPC of the transient quasi-steady states, we can build a physical picture about the ultrafast dynamic energy relaxation processes from the photocarriers to the optical phonons (the A'_1 mode here). In comparison with the EPC constant λ, the EPC energy exchange rate P can be used to evaluate the dynamic time-resolved coupling strength between the photoexcited electrons and the lattice on the ultrafast time scale.[22,23,52] Here we evaluate the time-dependent energy exchange rate P from the photocarriers to the A'_1 phonon mode using the non-equilibrium electronic occupation and EPC matrix elements:

https://doi.org/10.1021/acs.nanolett.2c01105
Nano Lett. 2022, 22, 4800−4806

$$P \equiv \frac{\partial E}{\partial t} = 4\pi\omega_{qv}\sum_{k,i,j}\{|g_{ij}^{qv}(k,k)|^2[f_{ik}(1-f_{jk})(n_{qv}+1) - (1-f_{ik})f_{jk}n_{qv}]\delta(E_{ik}-E_{jk}-\hbar\omega_{qv})\} \quad (5)$$

where ω_{qv} is the phonon frequency and $g_{ij}^{qv}(k,k)$ is the EPC matrix element. f_{nk} and n_{qv} denote the occupations of electrons and phonons, respectively. E_{ik} and E_{jk} are eigenvalues with the wave vector k and band index i,j. Similar to the previous analyses, the contribution of intraband transitions dominates.

Figure 4 displays the time-daependent evolution of the energy exchange rate P under illumination of a laser pulse.

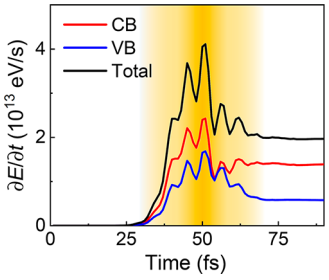

Figure 4. Time evolution of EPC energy exchange rate P after photoexcitation under the laser pulse (2.5 mJ/cm^2). The color gradient region schematically shows the variation of the intensity of the laser electric field. The black line indicates the total energy exchange rate between electrons and phonons, and red and blue lines represent the contributions from the conduction band and valence band, respectively.

When the laser pulse increases, the energy exchange rate P rapidly increases with a oscillation period of $T \approx 5$ fs, which is ascribed to the growing photoexcited electronic occupation. Then it decays to the steady value $P \approx 2 \times 10^{13}$ eV/s shortly after the laser pulse vanishes. The conduction band contributes over 70% of the EPC energy exchange rate P, mainly because the deformation potential of the conduction band is larger than that of the valence band (Note 9 in the Supporting Information). Our results correspond to the early stages of relaxation processes under experimental conditions, when photoexcited electrons/holes couple with the high-energy optical phonon modes.[53] If one assumes that the given hot electrons are interacting with thermal hot phonons instead of the nonthermal phonons, the EPC will be influenced by phonon−phonon interactions and the linear superposition of various phonon modes.

According to these analyses of transient EPC, we suggest that the investigation of nonequilibrium EPC could provide a route to engineer ultrafast devices. By photoexciting electrons into antibonding orbitals, one can effectively tune the deformation potential by laser pulses. This provides the opportunity to design the optical control strategies for photoinduced phase transitions or even light-enhanced phonon-mediated superconductivity.[54] We anticipate a prominent change in the deformation potential and a limited phase space at the early stages of photoexcitation that suppresses the decay of optical phonons to acoustic phonons will trigger a practical long-lived quantum state to play a role in ultrafast switching devices, photocatalysis, and other real-world applications.

Note that the long-range Coulomb forces are absent in all of our investigations, while the dynamic screening of Fröhlich electron−phonon coupling may also influence the EPC in MoS_2, which goes beyond the capability of DFT.[49] Miller et al. showed that Fröhlich exciton−LO phonon scattering can be tuned by electronic doping thanks to an electron−impurity interaction.[55] We also note some works on the calculation of Fröhlich EPC in doped semiconductors by means of effectively estimated dielectric constants.[56] The photoinduced screening of a Fröhlich interaction is of great interest, posing new challenges for tools on many-body interactions. Recent developments in time-dependent GW equations provide further opportunities in this aspect.[57,58]

In conclusion, we have investigated the variation of the matrix element g, the overall constant λ, and the energy exchange rate P of electron−phonon couplings under laser excitation within the framework of real-time TDDFT. We extract the time-dependent amplitude of energy bands and atomic displacements; thus, the out-of-equilibrium EPC matrix elements and electronic occupations can be derived. We found that photoexcited carriers can change the electronic screening, thus modulating the PES of the A'_1 mode in 1L-MoS_2 to alter the EPC matrix elements. This effect, in combination with the increased carrier density, leads to the enhancement in EPC upon photoexcitation. In addition, we evaluated the energy exchange rate P from laser excited electrons to high-energy optical phonons, which is deemed to be the main process during the early stage of the relaxation process under photoexcitation. Our work paves new ways to understand phonon-mediated nonequilibrium phenomena and strips out the the early state of energy relaxation processes from photoexcited electrons to optical phonons.

■ ASSOCIATED CONTENT

Supporting Information

The Supporting Information is available free of charge at https://pubs.acs.org/doi/10.1021/acs.nanolett.2c01105.

Detailed methods, analysis of EPC matrix elements, electronic screening, and discussion of the potential energy surface (PDF)

■ AUTHOR INFORMATION

Corresponding Author

Sheng Meng − *Beijing National Laboratory for Condensed Matter Physics and Institute of Physics, Chinese Academy of Sciences, Beijing 100190, People's Republic of China; School of Physical Sciences, University of Chinese Academy of Sciences, Beijing 100190, People's Republic of China; Songshan Lake Materials Laboratory, Dongguan, Guangdong 523808, People's Republic of China;* orcid.org/0000-0002-1553-1432; Email: smeng@iphy.ac.cn

Authors

Xin-Bao Liu − *Beijing National Laboratory for Condensed Matter Physics and Institute of Physics, Chinese Academy of Sciences, Beijing 100190, People's Republic of China; School of Physical Sciences, University of Chinese Academy of Sciences, Beijing 100190, People's Republic of China*

Shi-Qi Hu − *Beijing National Laboratory for Condensed Matter Physics and Institute of Physics, Chinese Academy of Sciences, Beijing 100190, People's Republic of China; School*

https://doi.org/10.1021/acs.nanolett.2c01105
Nano Lett. 2022, 22, 4800−4806

of Physical Sciences, University of Chinese Academy of Sciences, Beijing 100190, People's Republic of China

Daqiang Chen − *Beijing National Laboratory for Condensed Matter Physics and Institute of Physics, Chinese Academy of Sciences, Beijing 100190, People's Republic of China; School of Physical Sciences, University of Chinese Academy of Sciences, Beijing 100190, People's Republic of China*

Mengxue Guan − *Beijing National Laboratory for Condensed Matter Physics and Institute of Physics, Chinese Academy of Sciences, Beijing 100190, People's Republic of China; School of Physical Sciences, University of Chinese Academy of Sciences, Beijing 100190, People's Republic of China;* orcid.org/0000-0002-6987-4211

Qing Chen − *Beijing National Laboratory for Condensed Matter Physics and Institute of Physics, Chinese Academy of Sciences, Beijing 100190, People's Republic of China; School of Physical Sciences, University of Chinese Academy of Sciences, Beijing 100190, People's Republic of China*

Complete contact information is available at: https://pubs.acs.org/10.1021/acs.nanolett.2c01105

Author Contributions

[‖]X.-B.L. and S.-Q.H. contributed equally.

Notes

The authors declare no competing financial interest.

■ ACKNOWLEDGMENTS

We acknowledge helpful discussions with Yutao Jiang. This work was partially supported by the MOST (grant 2021YFA1400200), NSFC (grants 12025407 and 11934003), and CAS (XDB330301).

■ REFERENCES

(1) Grimvall, G. *The Electron-phonon Interaction in Metals*; North-Holland Publishing Company: 1981.

(2) Duan, H. G.; Tiwari, V.; Jha, A.; Berdiyorov, G. R.; Akimov, A.; Vendrell, O.; Nayak, P. K.; Snaith, H. J.; Thorwart, M.; Li, Z.; Madjet, M. E.; Miller, R. J. D. Photoinduced Vibrations Drive Ultrafast Structural Distortion in Lead Halide Perovskite. *J. Am. Chem. Soc.* **2020**, *142* (39), 16569−16578.

(3) Luo, D.; Su, R.; Zhang, W.; Gong, Q.; Zhu, R. Minimizing non-radiative recombination losses in perovskite solar cells. *Nat. Rev. Mater.* **2020**, *5* (1), 44−60.

(4) Puppin, M.; Polishchuk, S.; Colonna, N.; Crepaldi, A.; Dirin, D. N.; Nazarenko, O.; De Gennaro, R.; Gatti, G.; Roth, S.; Barillot, T.; Poletto, L.; Xian, R. P.; Rettig, L.; Wolf, M.; Ernstorfer, R.; Kovalenko, M. V.; Marzari, N.; Grioni, M.; Chergui, M. Evidence of Large Polarons in Photoemission Band Mapping of the Perovskite Semiconductor $CsPbBr_3$. *Phys. Rev. Lett.* **2020**, *124* (20), 206402.

(5) Nicholson, C. W.; Lücke, A.; Schmidt, W. G.; Puppin, M.; Rettig, L.; Ernstorfer, R.; Wolf, M. Beyond the molecular movie: Dynamics of bands and bonds during a photoinduced phase transition. *Science* **2018**, *362* (6416), 821−825.

(6) Maklar, J.; Windsor, Y. W.; Nicholson, C. W.; Puppin, M.; Walmsley, P.; Esposito, V.; Porer, M.; Rittmann, J.; Leuenberger, D.; Kubli, M.; Savoini, M.; Abreu, E.; Johnson, S. L.; Beaud, P.; Ingold, G.; Staub, U.; Fisher, I. R.; Ernstorfer, R.; Wolf, M.; Rettig, L. Nonequilibrium charge-density-wave order beyond the thermal limit. *Nat. Commun.* **2021**, *12* (1), 2499.

(7) Hase, M.; Kitajima, M.; Nakashima, S.; Mizoguchi, K. Dynamics of coherent anharmonic phonons in bismuth using high density photoexcitation. *Phys. Rev. Lett.* **2002**, *88* (6), 067401.

(8) Murray, E. D.; Fahy, S. First-principles calculation of femtosecond symmetry-breaking atomic forces in photoexcited bismuth. *Phys. Rev. Lett.* **2015**, *114* (5), 055502.

(9) O'Mahony, S. M.; Murphy-Armando, F.; Murray, E. D.; Querales-Flores, J. D.; Savic, I.; Fahy, S. Ultrafast Relaxation of Symmetry-Breaking Photo-Induced Atomic Forces. *Phys. Rev. Lett.* **2019**, *123* (8), 087401.

(10) Fausti, D.; Tobey, R. I.; Dean, N.; Kaiser, S.; Dienst, A.; Hoffmann, M. C.; Pyon, S.; Takayama, T.; Takagi, H.; Cavalleri, A. Light-Induced Superconductivity in a Stripe-Ordered Cuprate. *Science* **2011**, *331* (6014), 189−191.

(11) Budden, M.; Gebert, T.; Buzzi, M.; Jotzu, G.; Wang, E.; Matsuyama, T.; Meier, G.; Laplace, Y.; Pontiroli, D.; Riccò, M.; Schlawin, F.; Jaksch, D.; Cavalleri, A. Evidence for metastable photo-induced superconductivity in K_3C_{60}. *Nat. Phys.* **2021**, *17* (5), 611−618.

(12) Lian, C.; Zhang, S.-J.; Hu, S.-Q.; Guan, M.-X.; Meng, S. Ultrafast charge ordering by self-amplified exciton−phonon dynamics in $TiSe_2$. *Nat. Commun.* **2020**, *11* (1), 43.

(13) Zong, A.; Dolgirev, P. E.; Kogar, A.; Su, Y.; Shen, X.; Straquadine, J. A. W.; Wang, X.; Luo, D.; Kozina, M. E.; Reid, A. H.; Li, R.; Yang, J.; Weathersby, S. P.; Park, S.; Sie, E. J.; Jarillo-Herrero, P.; Fisher, I. R.; Wang, X.; Demler, E.; Gedik, N. Role of Equilibrium Fluctuations in Light-Induced Order. *Phys. Rev. Lett.* **2021**, *127* (22), 227401.

(14) Stojchevska, L.; Vaskivskyi, I.; Mertelj, T.; Kusar, P.; Svetin, D.; Brazovskii, S.; Mihailovic, D. Ultrafast Switching to a Stable Hidden Quantum State in an Electronic Crystal. *Science* **2014**, *344* (6180), 177−180.

(15) Richter, J. M.; Branchi, F.; Valduga de Almeida Camargo, F.; Zhao, B.; Friend, R. H.; Cerullo, G.; Deschler, F. Ultrafast carrier thermalization in lead iodide perovskite probed with two-dimensional electronic spectroscopy. *Nat. Commun.* **2017**, *8* (1), 376.

(16) Shin, D.; Sato, S. A.; Hübener, H.; De Giovannini, U.; Park, N.; Rubio, A. Dynamical amplification of electric polarization through nonlinear phononics in 2D SnTe. *npj Comput. Mater.* **2020**, *6* (1), 182.

(17) Song, Z.; Wang, L.-W. Electron-phonon coupling induced intrinsic Floquet electronic structure. *npj Quantum Mater.* **2020**, *5* (1), 77.

(18) Topp, G. E.; Tancogne-Dejean, N.; Kemper, A. F.; Rubio, A.; Sentef, M. A. All-optical nonequilibrium pathway to stabilising magnetic Weyl semimetals in pyrochlore iridates. *Nat. Commun.* **2018**, *9* (1), 4452.

(19) Disa, A. S.; Nova, T. F.; Cavalleri, A. Engineering crystal structures with light. *Nat. Phys.* **2021**, *17* (10), 1087−1092.

(20) de la Torre, A.; Kennes, D. M.; Claassen, M.; Gerber, S.; McIver, J. W.; Sentef, M. A. Colloquium: Nonthermal pathways to ultrafast control in quantum materials. *Rev. Mod. Phys.* **2021**, *93* (4), 041002.

(21) Allen, P. B. Theory of thermal relaxation of electrons in metals. *Phys. Rev. Lett.* **1987**, *59* (13), 1460−1463.

(22) Lin, Z.; Zhigilei, L. V.; Celli, V. Electron-phonon coupling and electron heat capacity of metals under conditions of strong electron-phonon nonequilibrium. *Phys. Rev. B* **2008**, *77* (7), 075133.

(23) Sadasivam, S.; Chan, M. K. Y.; Darancet, P. Theory of Thermal Relaxation of Electrons in Semiconductors. *Phys. Rev. Lett.* **2017**, *119* (13), 136602.

(24) Waldecker, L.; Bertoni, R.; Ernstorfer, R.; Vorberger, J. Electron-Phonon Coupling and Energy Flow in a Simple Metal beyond the Two-Temperature Approximation. *Phys. Rev. X* **2016**, *6* (2), 021003.

(25) Novko, D.; Caruso, F.; Draxl, C.; Cappelluti, E. Ultrafast Hot Phonon Dynamics in MgB_2 Driven by Anisotropic Electron-Phonon Coupling. *Phys. Rev. Lett.* **2020**, *124* (7), 077001.

(26) Tong, X.; Bernardi, M. Toward precise simulations of the coupled ultrafast dynamics of electrons and atomic vibrations in materials. *Phys. Rev. Res.* **2021**, *3* (2), 023072.

(27) Caruso, F. Nonequilibrium Lattice Dynamics in Monolayer MoS_2. *J. Phys. Chem. Lett.* **2021**, *12* (6), 1734−1740.

(28) Giustino, F. Electron-phonon interactions from first principles. *Rev. Mod. Phys.* **2017**, *89* (1), 015003.

(29) Kennes, D. M.; Wilner, E. Y.; Reichman, D. R.; Millis, A. J. Transient superconductivity from electronic squeezing of optically pumped phonons. *Nat. Phys.* **2017**, *13* (5), 479−483.
(30) Sentef, M. A. Light-enhanced electron-phonon coupling from nonlinear electron-phonon coupling. *Phys. Rev. B* **2017**, *95* (20), 205111.
(31) Sous, J.; Kloss, B.; Kennes, D. M.; Reichman, D. R.; Millis, A. J. Phonon-induced disorder in dynamics of optically pumped metals from nonlinear electron-phonon coupling. *Nat. Commun.* **2021**, *12* (1), 5803.
(32) Gerber, S.; Yang, S. L.; Zhu, D.; Soifer, H.; Sobota, J. A.; Rebec, S.; Lee, J. J.; Jia, T.; Moritz, B.; Jia, C.; Gauthier, A.; Li, Y.; Leuenberger, D.; Zhang, Y.; Chaix, L.; Li, W.; Jang, H.; Lee, J. S.; Yi, M.; Dakovski, G. L.; Song, S.; Glownia, J. M.; Nelson, S.; Kim, K. W.; Chuang, Y. D.; Hussain, Z.; Moore, R. G.; Devereaux, T. P.; Lee, W. S.; Kirchmann, P. S.; Shen, Z. X. Femtosecond electron-phonon lock-in by photoemission and x-ray free-electron laser. *Science* **2017**, *357* (6346), 71−75.
(33) Na, M. X.; Mills, A. K.; Boschini, F.; Michiardi, M.; Nosarzewski, B.; Day, R. P.; Razzoli, E.; Sheyerman, A.; Schneider, M.; Levy, G.; Zhdanovich, S.; Devereaux, T. P.; Kemper, A. F.; Jones, D. J.; Damascelli, A. Direct determination of mode-projected electron-phonon coupling in the time domain. *Science* **2019**, *366* (6470), 1231−1236.
(34) Hein, P.; Jauernik, S.; Erk, H.; Yang, L.; Qi, Y.; Sun, Y.; Felser, C.; Bauer, M. Mode-resolved reciprocal space mapping of electron-phonon interaction in the Weyl semimetal candidate Td-WTe_2. *Nat. Commun.* **2020**, *11* (1), 2613.
(35) De Giovannini, U.; Hubener, H.; Sato, S. A.; Rubio, A. Direct Measurement of Electron-Phonon Coupling with Time-Resolved ARPES. *Phys. Rev. Lett.* **2020**, *125* (13), 136401.
(36) Runge, E.; Gross, E. K. U. Density-Functional Theory for Time-Dependent Systems. *Phys. Rev. Lett.* **1984**, *52* (12), 997−1000.
(37) Ma, W.; Zhang, J.; Yan, L.; Jiao, Y.; Gao, Y.; Meng, S. Recent progresses in real-time local-basis implementation of time dependent density functional theory for electron−nucleus dynamics. *Comput. Mater. Sci.* **2016**, *112*, 478−486.
(38) Lian, C.; Guan, M.; Hu, S.; Zhang, J.; Meng, S. Photoexcitation in Solids: First-Principles Quantum Simulations by Real-Time TDDFT. *Adv. Theor. Simul.* **2018**, *1* (8), 1800055.
(39) You, P.; Chen, D.; Lian, C.; Zhang, C.; Meng, S. First-principles dynamics of photoexcited molecules and materials towards a quantum description. *WIREs Comput. Mol. Sci.* **2021**, *11* (2), No. e1492.
(40) Liu, F.; Ziffer, M. E.; Hansen, K. R.; Wang, J.; Zhu, X. Direct Determination of Band-Gap Renormalization in the Photoexcited Monolayer MoS_2. *Phys. Rev. Lett.* **2019**, *122* (24), 246803.
(41) Marini, G.; Calandra, M. Lattice dynamics of photoexcited insulators from constrained density-functional perturbation theory. *Phys. Rev. B* **2021**, *104* (14), 144103.
(42) Grubišić Čabo, A.; Miwa, J. A.; Grønborg, S. S.; Riley, J. M.; Johannsen, J. C.; Cacho, C.; Alexander, O.; Chapman, R. T.; Springate, E.; Grioni, M.; Lauritsen, J. V.; King, P. D. C.; Hofmann, P.; Ulstrup, S. Observation of Ultrafast Free Carrier Dynamics in Single Layer MoS_2. *Nano Lett.* **2015**, *15* (9), 5883−5887.
(43) Wierzbowska, M.; de Gironcoli, S.; Giannozzi, P. *Origins of low- and high-pressure discontinuities of T_c in niobium*. 2005, arXiv.org, arXiv:cond-mat/0504077, https://arxiv.org/abs/cond-mat/0504077 (accessed October 15, 2021).
(44) Tangney, P.; Fahy, S. Density-functional theory approach to ultrafast laser excitation of semiconductors: Application to the A_1 phonon in tellurium. *Phys. Rev. B* **2002**, *65* (5), 054302.
(45) Tangney, P.; Fahy, S. Calculations of the A_1 Phonon Frequency in Photoexcited Tellurium. *Phys. Rev. Lett.* **1999**, *82* (21), 4340−4343.
(46) Sohier, T.; Ponomarev, E.; Gibertini, M.; Berger, H.; Marzari, N.; Ubrig, N.; Morpurgo, A. F. Enhanced Electron-Phonon Interaction in Multivalley Materials. *Phys. Rev. X* **2019**, *9* (3), 031019.
(47) Giannozzi, P.; Andreussi, O.; Brumme, T.; Bunau, O.; Buongiorno Nardelli, M.; Calandra, M.; Car, R.; Cavazzoni, C.; Ceresoli, D.; Cococcioni, M.; Colonna, N.; Carnimeo, I.; Dal Corso, A.; de Gironcoli, S.; Delugas, P.; DiStasio, R. A.; Ferretti, A.; Floris, A.; Fratesi, G.; Fugallo, G.; Gebauer, R.; Gerstmann, U.; Giustino, F.; Gorni, T.; Jia, J.; Kawamura, M.; Ko, H. Y.; Kokalj, A.; Küçükbenli, E.; Lazzeri, M.; Marsili, M.; Marzari, N.; Mauri, F.; Nguyen, N. L.; Nguyen, H. V.; Otero-de-la-Roza, A.; Paulatto, L.; Poncé, S.; Rocca, D.; Sabatini, R.; Santra, B.; Schlipf, M.; Seitsonen, A. P.; Smogunov, A.; Timrov, I.; Thonhauser, T.; Umari, P.; Vast, N.; Wu, X.; Baroni, S. Advanced capabilities for materials modelling with Quantum ESPRESSO. *J. Phys.: Condens. Matter* **2017**, *29* (46), 465901.
(48) Poncé, S.; Margine, E. R.; Verdi, C.; Giustino, F. EPW: Electron−phonon coupling, transport and superconducting properties using maximally localized Wannier functions. *Comput. Phys. Commun.* **2016**, *209*, 116−133.
(49) Verdi, C.; Caruso, F.; Giustino, F. Origin of the crossover from polarons to Fermi liquids in transition metal oxides. *Nat. Commun.* **2017**, *8*, 15769.
(50) Beaulieu, S.; Dong, S.; Tancogne-Dejean, N.; Dendzik, M.; Pincelli, T.; Maklar, J.; Xian, R. P.; Sentef Michael, A.; Wolf, M.; Rubio, A.; Rettig, L.; Ernstorfer, R. Ultrafast dynamical Lifshitz transition. *Sci. Adv.* **2021**, *7* (17), No. eabd9275.
(51) Baykusheva, D. R.; Jang, H.; Husain, A. A.; Lee, S.; TenHuisen, S. F. R.; Zhou, P.; Park, S.; Kim, H.; Kim, J.-K.; Kim, H.-D.; Kim, M.; Park, S.-Y.; Abbamonte, P.; Kim, B. J.; Gu, G. D.; Wang, Y.; Mitrano, M. Ultrafast Renormalization of the On-Site Coulomb Repulsion in a Cuprate Superconductor. *Phys. Rev. X* **2022**, *12* (1), 011013.
(52) Medvedev, N.; Milov, I. Electron-phonon coupling in metals at high electronic temperatures. *Phys. Rev. B* **2020**, *102* (6), 064302.
(53) Obergfell, M.; Demsar, J. Tracking the Time Evolution of the Electron Distribution Function in Copper by Femtosecond Broadband Optical Spectroscopy. *Phys. Rev. Lett.* **2020**, *124* (3), 037401.
(54) Guan, M.-X.; Liu, X.-B.; Chen, D.-Q.; Li, X.-Y.; Qi, Y.-P.; Yang, Q.; You, P.-W.; Meng, S. Optical Control of Multistage Phase Transition via Phonon Coupling in MoTe2. *Phys. Rev. Lett.* **2022**, *128* (1), 015702.
(55) Miller, B.; Lindlau, J.; Bommert, M.; Neumann, A.; Yamaguchi, H.; Holleitner, A.; Hogele, A.; Wurstbauer, U. Tuning the Frohlich exciton-phonon scattering in monolayer MoS2. *Nat. Commun.* **2019**, *10* (1), 807.
(56) Macheda, F.; Barone, P.; Mauri, F. *Fröhlich electron-phonon interaction and LO-TO splitting in doped semiconductors*. 2022, arXiv.org, arXiv:2202.02835, https://arxiv.org/abs/2202.02835 (accessed February 20, 2022).
(57) Karlsson, D.; van Leeuwen, R.; Pavlyukh, Y.; Perfetto, E.; Stefanucci, G. Fast Green's Function Method for Ultrafast Electron-Boson Dynamics. *Phys. Rev. Lett.* **2021**, *127* (3), 036402.
(58) Perfetto, E.; Pavlyukh, Y.; Stefanucci, G. Real-Time GW: Toward an Ab Initio Description of the Ultrafast Carrier and Exciton Dynamics in Two-Dimensional Materials. *Phys. Rev. Lett.* **2022**, *128* (1), 016801.

https://doi.org/10.1021/acs.nanolett.2c01105
Nano Lett. 2022, 22, 4800−4806